Table 1 Jet-engine spike and Trichel pulse comparison

Parameter	Jet engine exhaust	Trichel pulse
Polarity	Positive	Positive
Shape	Distinctive step on trailing edge	Distinctive step on trailing edge
Rise time	2 - 4 ns	< 10 ns
Net charge	0.1 - 10 nC	0.01 - 10 nC
Width	0.2 - 5 μs	0.01 - 5 μs
Repetition	Spike showers repetitive in nature - 10^5 - 10^6 Hz Increases then decreases in frequency	Increasing frequency with increasing applied potential 100 - 10^6 Hz
Amplitude	Showers: first decreasing then increasing	Increasing then decreasing with applied potential

Evidence for Charged Clouds

In all our simulated experiments, Trichel pulses were obtained using a flat-plate anode. There is no obvious equivalent to such an anode in an engine exhaust/probe situation. Hence, a charged gas eddy or clouds associated with high electrical potentials must be postulated. Such clouds could be expected to move past the probe at the mean flow velocity. This charged cloud would not have to impact the probe, but should pass sufficiently close to induce probe-tip electric fields above the onset level.

The engine probe shower data support this postulate (Fig. 1b). These data show that the pulses at the start and finish of a shower have lower pulse rates and higher amplitudes than the pulses midway in the shower. These data are interpreted to indicate that the charged cloud is moving past the probe. As the cloud approaches and then recedes from the probe, the electric field at the probe tip increases, reaches a maximum, and then decreases. This phenomenon corresponds to Trichel pulse response as a function of applied voltage electric field; when the frequency exceeds 50 kHz, increasing the anode voltage increases the pulse rate and decreases the amplitude.

Charged-cloud properties can be estimated from the jet-engine spike probe data and our experimental results using the following assumptions. 1) The charged cloud moves with the jet exhaust gas exit velocity, ~ 305 m/s; 2) The cloud has a spherical shape. 3) The Trichel pulse onset potential for the blunt nose 0.563-cm AFFDL probe is 18 kV (where the value at room temperature was 26 kV and 12 kV in a propane flame). The cloud diameter is 15 cm based on the duration of a pulse shower, 500 μs (Fig. 1b), and the capacitance is 10 pF (for a sphere one body diameter above a ground plane). The net charge in the cloud is hence 180 nC with a resultant net charge density of 6×10^8 cm^{-3} and an electrostatic energy of 1.6 mJ. The cloud polarity is positive because an opposite sign would cause an anode corona at the probe tip whose properties would be far different from those of negative corona Trichel pulses. In particular, positive coronas are not known to display the well-defined repetition rates with frequencies up to several megahertz.

The sources of charged clouds have not been determined. Statistical evidence[3] indicates that they are related to certain engine failure modes and that their presence can be a warning of imminent engine failure. Three postulated mechanisms for producing charged clouds have been suggested,[1,2] particulate cloud, spray charging, and boundary-layer fluid accumulation.

Conclusions

The electrostatic probe spike signals observed in a jet-engine exhaust are deduced to be a particular form of negative electrical corona discharge known as Trichel pulses. Analyses of the spike shower data and known properties of Trichel pulses infer that the spike signals are induced by a positive, high-potential cloud which moves past the probe.

Acknowledgment

This work was supported by United States Air Force Flight Dynamics Laboratory, Contract No. F33615-74-C-3091.

References

[1] Shaeffer, J. F. and Peng, T. C., "High Potential Clouds in Jet Engine Exhausts," AIAA Paper 76-397, San Diego, Calif., 1976.

[2] Sajben, M., Peng, T. C., and Shaeffer, J. F., "Evaluation of Experiments using Electrostatic Probes to Detect Imminent Failure of Jet-Engine Gas-Path Components," Air Force Flight Dynamics Lab, Wright Patterson, AFB, Ohio, AFFDL TR-75-74, July 1975.

[3] Couch, R. P. and Rossbach, D. R., "Sensing Jet Engine Performance and Incipient Failure with Electrostatic Probes," Air Force Dynamics Lab, Wright Patterson, AFB, Ohio, AFFDL TR-71-173, Dec. 1972.

Velocity-Temperature Relations in Turbulent Boundary Layers with Nonunity Prandtl Numbers

D. L. Whitfield* and M. D. High†
ARO, Inc., Arnold Air Force Station, Tenn.

Nomenclature

A = $(\gamma-1)M_\infty^2$
f = function defined by Eq. (8)
H = specific total enthalpy
$\bar{H}_\infty$ = $H_\infty/h_\infty = 1+A/2$
h = specific enthalpy
$\bar{h}$ = h/h_∞
$\bar{h}_0$ = zeroth-order $\bar{h}$
$\bar{h}_1$ = first-order $\bar{h}$
k = molecular thermal conductivity
k_t = eddy thermal conductivity
M = Mach number
m = $\bar{u}=\eta^{1/m}$, used herein as $m=7$
Pr_m = mixed Prandtl number, $c_p(\mu+\mu_t)/(k+k_t)$
r = recovery factor, $r=(T_{aw}-T_\infty)/(T_{0,\infty}-T_\infty)$
T = mean static temperature
T_0 = local total temperature
$\bar{T}$ = $(T_0-T_w)/(T_{0,\infty}-T_w)$
$\bar{u}$ = mean flow velocity
u = u/u_∞
u_τ = $u/(\tau_w/\rho_w)^{1/2}$
Y = distance normal to surface
α = $(5/2)m$
γ = ratio of specific heats
Δ = defined by Eq. (10) for constant temperature wall and by Eq. (13) for an adiabatic wall
δ = boundary-layer thickness
ϵ = $1-Pr_m$
η = Y/δ
μ = molecular viscosity
μ_t = eddy viscosity

Presented as Paper 76-411 at the AIAA 9th Fluid and Plasma Dynamics Conference, San Diego, Calif., July 14-16, 1976; submitted July 23, 1976; revision received Nov. 24, 1976.

Index category: Boundary Layers and Convective Heat Transfer – Turbulent.

*Supervisor, Analysis Section, 16T/S Projects Branch, Propulsion Wind-Tunnel Facility. Member AIAA.

†Assistant Branch Manager, 16T/S Projects Branch, Propulsion Wind-Tunnel Facility. Associate Fellow AIAA.

ζ = defined by Eq. (9) for constant temperature wall and by Eq. (12) for an adiabatic wall
ρ = density
τ = total shear stress

Subscripts

aw = adiabatic wall
w = wall
∞ = boundary-layer edge

I. Introduction

ANALYTICAL expressions for temperature as a function of velocity in laminar and turbulent boundary layers were obtained by Busemann and Crocco as summarized by Schlichting.[1] These expressions are convenient and have been used extensively. The simple expressions of Busemann and Crocco are independent of the shear stress distribution in the boundary layer as a consequence of considering unity Prandtl number.

Van Driest[2] investigated this problem by considering a variable Prandtl number across a turbulent boundary layer. He obtained a general expression for temperature as a function of velocity in adiabatic flow which required Prandtl number and shear stress distributions across the boundary layer. Some numerical approximations were required, but van Driest's analysis illustrated the effect of Prandtl number and showed that the local total temperature must exceed the freestream total temperature near the edge of the boundary layer (overshoot) for adiabatic flow with nonunity Prandtl number.

The objective of the present work was to obtain analytical expressions for temperature as a function of velocity in adiabatic or constant wall temperature turbulent boundary-layer flows with constant but nonunity Prandtl numbers. The approach was to use the equation resulting from combining the boundary-layer momentum and energy equations and model the Reynolds stress by assuming it proportional to the local turbulent kinetic energy in the boundary layer. A second-order, nonlinear, ordinary differential equation results, for which zeroth- and first-order perturbation solutions were obtained for temperature as a function of velocity in terms of the small parameter $\epsilon = 1 - Pr_m$. Crocco's result is recovered identically by the zeroth-order solution. The additional first-order solution permits, for example, the calculation of total temperature overshoot in an adiabatic boundary layer which the Crocco or modified Crocco results cannot predict.

II. Analysis

Basic Equation

The basic equation is obtained by combining the boundary-layer momentum and energy equations as a consequence of the proposition that temperature is a function of velocity only. Schlichting[1] shows that this proposition is correct if: 1) the pressure and wall temperature gradients are zero and the Prandtl number unity, or 2) the wall is adiabatic and Prandtl number unity for nonzero pressure gradient. Because the present approach is to obtain solutions for Prandtl numbers near unity, it is assumed that the solutions are approximately correct for conditions 1 and 2 for near unity Prandtl numbers.

The boundary-layer equations considered consisted of both the laminar and turbulent contributions to viscosity and thermal conductivity. van Driest[2] considered these same equations, and obtained for constant mixed Prandtl number Pr_m the expression

$$\frac{d^2\bar{h}}{d\bar{u}^2} + (1 - Pr_m)\frac{1}{\tau}\frac{d\tau}{d\bar{u}}\frac{d\bar{h}}{d\bar{u}} + Pr_m(\gamma - 1)M_\infty{}^2 = 0 \qquad (1)$$

In Ref. 3 an analytical approximation was made for the distribution of turbulent kinetic energy across the boundary layer. Using this approximation, and the assumption that the Reynolds stress is proportional to the local turbulent kinetic energy, the expression

$$\tau = u_\tau{}^2 \rho \exp(-4\eta^{5/2}) \qquad (2)$$

is obtained as an approximation for the total shear stress distribution across the boundary layer. Using Eq. (2) in Eq. (1), one term remains which contains η rather than the variable u. In order to eliminate η, it was assumed that $\bar{u} = \eta^{1/m}$ for this term. This assumption is thought to introduce little error, because near the wall where this power-law assumption is particularly bad, the total shear is nearly constant and the shear stress term in Eq. (1) is small. This assumption, however, is justified only by the final results. With Eq. (2) used for τ in Eq. (1), noting that the flow is compressible, and using the perfect gas equation of state, the basic equation to be solved can be written as

$$\bar{h}\frac{d^2\bar{h}}{d\bar{u}^2} - \epsilon\left(4\alpha\bar{u}^{\alpha-1}\bar{h} + \frac{d\bar{h}}{d\bar{u}}\right)\frac{d\bar{h}}{d\bar{u}} + (1-\epsilon)A\bar{h} = 0 \qquad (3)$$

Constant Wall Temperature Solution

Equation (3) is a second-order, nonlinear ordinary differential equation for $\bar{h}(\bar{u})$. Zeroth- and first-order perturbation solutions were obtained in terms of the small parameter, ϵ. The boundary conditions for the constant wall temperature problem are $\bar{h}(0) = \bar{h}_w$ and $\bar{h}(1) = 1$. Assuming a solution of the form

$$\bar{h}(\bar{u}) = \bar{h}_0(\bar{u}) + \epsilon\bar{h}_1(\bar{u}) + \ldots \qquad (4)$$

one obtains to zeroth order

$$d^2\bar{h}_0/d\bar{u}^2 = -A \qquad (5)$$

and to first order

$$\frac{d^2\bar{h}_1}{d\bar{u}^2} = 4\alpha\bar{u}^{\alpha-1}\frac{d\bar{h}_0}{d\bar{u}} + \frac{1}{\bar{h}_0}\left(\frac{d\bar{h}_0}{d\bar{u}}\right)^2 + A \qquad (6)$$

The boundary conditions become $\bar{h}_0(0) = \bar{h}_w$, $\bar{h}_1(0) = 0$ and $\bar{h}_1(1) = 0$. The solution to Eq. (5) for the zeroth-order boundary conditions was used in Eq. (6) with the first-order boundary conditions to solve for $\bar{h}_1(u)$. The solution, up to first order is

$$\bar{h}(\bar{u}) = \bar{h}_w + (\bar{H}_\infty - \bar{h}_w)\bar{u} - \frac{A}{2}\bar{u}^2 + \epsilon\left[\frac{4\alpha A\bar{u}}{(\alpha+1)(\alpha+2)}\left(1 - \bar{u}^{\alpha+1}\right) - \frac{4(\bar{H}_\infty - \bar{h}_w)\bar{u}}{(\alpha+1)}(1 - \bar{u}^\alpha) + \frac{A}{2}\bar{u}(1-\bar{u}) + (1-\bar{u})f(0) + \bar{u}f(1) - f(\bar{u})\right] \qquad (7)$$

where

$$f(\bar{u}) = (\Delta/A)\left[(\zeta - \Delta)\ln|\zeta - \Delta| - (\zeta + \Delta)\ln|\zeta + \Delta|\right] \qquad (8)$$

$$\zeta = \bar{H}_\infty - \bar{h}_w - A\bar{u} \qquad (9)$$

and

$$\Delta = [2A\bar{h}_w + (\bar{H}_\infty - \bar{h}_w)^2]^{1/2} \qquad (10)$$

Adiabatic-Wall Solution

The boundary conditions for the adiabatic wall problem are

$$\left.\frac{d\bar{h}}{d\bar{u}}\right|_{\bar{u}=0} = 0$$

and $\bar{h}(1)=1$. The solution procedure is the same as that for the constant wall temperature case, and the solution is

$$\bar{h}(\bar{u})=1+\frac{A}{2}(1-\bar{u}^2)+\epsilon\left[\frac{4\alpha A}{(\alpha+1)(\alpha+2)}\left(1-\bar{u}^{\alpha+2}\right)\right.$$

$$\left.+\frac{A}{2}(1-\bar{u}^2)+f(1)-f(\bar{u})\right] \tag{11}$$

where $f(\bar{u})$ is the same as Eq. (8) above but ζ and Δ now are defined as

$$\zeta=-A\bar{u} \tag{12}$$

and

$$\Delta=(2A\bar{H}_\infty)^{1/2} \tag{13}$$

III. Results and Comparisons

To apply the present results it is necessary to know the Prandtl number. Because the variation in experimental recovery factors is less than in experimental Prandtl numbers, Pr_m was determined by assuming a constant recovery factor and calculating Pr_m using the adiabatic wall solution. The values of Pr_m determined in this way are presenting in Fig. 1 for recovery factors of 0.87, 0.88, 0.89, and 0.90. Available values of experimental recovery factors indicate a value of 0.88 as being representative, and this value was used for the present results.

The velocity-temperature results are presented in $\bar{u}-\bar{T}$ coordinates. It should be pointed out that $\bar{T}$ is a sensitive parameter. For example, consider an adiabatic surface in moderate supersonic flow. In this case, $\bar{T}=(T_0/T_{0,\infty}-T_{aw}/T_{0,\infty})/(1-T_{aw}/T_{0,\infty})$ and $(1-T_{aw}/T_{0,\infty})$ is of order 0.1. Therefore, if a $T_0/T_{0,\infty}$ overshoot of 1% occurs, the result is a 10% or order of magnitude more overshoot in $\bar{T}$. The adiabatic wall solution, Eq. (11), is presented in Fig. 2 for $\gamma=7/5$ and various M_∞ (rather than γ and M_∞, $A=(\gamma-1)M_\infty^2$ is the appropriate parameter). The overshoot in $\bar{T}$ decreases as M_∞ increases. Some experimental evidence of this trend is given in Ref. 3.

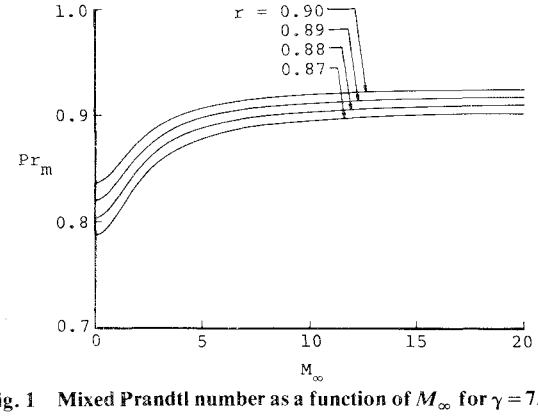

Fig. 1 Mixed Prandtl number as a function of M_∞ for $\gamma=7/5$.

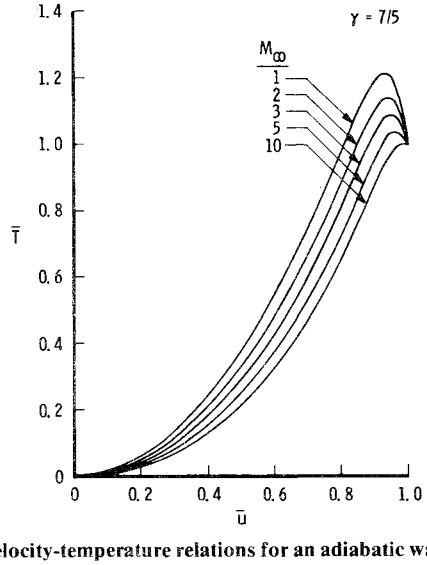

Fig. 2 Velocity-temperature relations for an adiabatic wall according to Eq. (11).

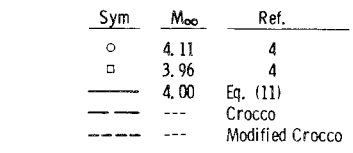

Flagged symbols are interpolated values in Ref. 4.

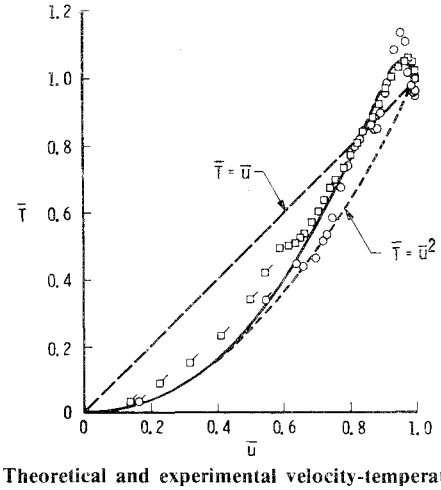

Fig. 3 Theoretical and experimental velocity-temperature relations for adiabatic flat plate.

Experimental adiabatic wall data of Gates[4] for $M_\infty \approx 4$ are compared with Eq. (11) in Fig. 3. Gates'[4] data were interpolated in the region between the wall and 0.025 in. from the wall and these results appear as flagged symbols in Fig. 3. Also included in Fig. 3 are the Crocco ($\bar{T}=\bar{u}$) and modified Crocco ($\bar{T}=\bar{u}^2$) results which, of course, do not describe the total temperature overshoot indicated by the experimental data or Eq. (11).

Comparisons with other experimental data (including nonadiabatic wall data) and numerical solutions of the complete boundary-layer equations are included in Ref. 3. The agreement obtained in Ref. 3 is considered good.

IV. Concluding Remarks

The present results contain the Crocco results as the zeroth-order solutions in Eqs. (7) and (11). The additional first-order solution permits, for example, the calculation of total temperature overshoot for the adiabatic wall case. The advantage of the present results is that analytical solutions were obtained as opposed to numerical solutions. These analytical results have been used at AEDC for various on-line and/or off-line data reduction requirements to reduce pitot pressure, laser doppler velocimeter, laser holographic interferometry, and split-film and hot-wire anemometer data.

References

[1]Schlichting, H., *Boundary Layer Theory*. fourth ed., McGraw-Hill, New York, 1960, Chap. XV.

[2]van Driest, E. R., "The Turbulent Boundary Layer with Variable Prandtl Number," *50 Jahre Grenzschichtferschung*, Friedr. Vieweg & Sohn, Braunschweight, 1955, pp. 257–271.

[3]Whitfield, D. L., "Analytical, Numerical, and Experimental Results on Turbulent Boundary Layers," AEDC-TR-76-62, 1976,

Arnold Engineering Development Center, Wright-Patterson AFB, Ohio.

[4]Gates, D. G., "Measurements of Upstream History Effects in Compressible Turbulent Boundary Layers," NOLTR 73-152, July 1973, Naval Ordnance Laboratory, Silver Spring, Md.

Target Intensity Enhancement for Repetitively Pulsed Laser Beams

J. Q. Lilly* and T. G. Miller†
U. S. Army Missile Research, Development, and Engineering Lab., U. S. Army Missile Command, Redstone Arsenal, Ala.

Introduction

A POSSIBLE method of minimizing the thermal blooming associated with the propagation of laser radiation through the atmosphere is to use repetitively pulsed lasers. This approach allows maintenance of high average power on target and, by optimizing the pulse width and intervals between pulses, permit convective clearing of the heated air between pulses. Results presented by Wallace and Lilly[1] showed that peak time-averaged intensities could be four or more times as great at low pulse repetition frequency (PRF) as continuous wave (CW) propagation at the same average power. At higher PRF, the peak intensities produced approach CW conditions and essentially no advantage is obtained. However, the results presented did not consider the effects of varying beam power or focal length.

In this paper, the dependence of peak intensity on target on the laser power level is theoretically investigated at low PRF for both focused and collimated beams. For the collimated case, the enhancement, or increase in peak intensity above the diffraction-limited (unbloomed) intensity, a result recently confirmed by experiment,[2] is investigated further. The results of Gebhardt et al.[2] showed that the peak intensity obtained for subsequent pulses could exceed the first pulse peak intensity by 20% or more. In this paper results are presented showing that this enhancement could reach 75% for optimum power beams.

Summary of Theory

The basic governing equations for thermal blooming of laser beams are the fluid dynamics conservation equations for determining atmospheric variables and the electromagnetic wave equations governing the laser energy distribution. To couple the solutions of these two basic equations, an additional equation relating the index of refraction and the air density is required.

For a repetitively pulsed laser beam consisting of a series of pulses of duration t_p separated by duration t_s where $t_p \ll t_s$, the solution for the density variation in the beam for the Nth pulse becomes

$$\left(\frac{\rho-\rho_\infty}{\rho_\infty}\right)^N = -\left(\frac{\gamma-1}{\gamma}\right)\frac{\alpha I_0 t_p}{p_\infty} \sum_{i=0}^{N-1} I_i\left[x-\frac{U_\infty t_s}{R_m}(N-i), y, z\right] \tag{1}$$

where

I_i = the intensity distribution of the ith pulse
ρ_∞ = the atmospheric ambient density
γ = the specific heat ratio
α = the absorption coefficient
I_0 = the beam peak intensity at $z=0$
p_∞ = the atmospheric pressure
x,y = the coordinates in the plane of the beam normalized with respect to R_m, the initial beam radius
z = the coordinate along the beam
U_∞ = the wind velocity transverse to the beam

The wind component can be modified to account for beam slewing, stagnation zones, etc. Additional terms accounting for pressure relaxation effects and single pulse blooming during time t_p have been neglected. Kinetic effects and bleaching are considered unimportant in the present analysis. The single term retained accounts for the overlapping effects of each succeeding pulse being transmitted through the air heated by the previous pulses. The shift, which produces overlapping between pulses is due to wind effects and is represented by $U_\infty t_s/R_m$. Defining one flow time as the time required for the wind to sweep across the beam at the aperture ($z=0$), the number of overlapping pulses contained within the beam is $2R_m/U_\infty t_s$. This quantity is defined as the pulses per flow time (PPFT) and specifies the number of previous pulses affecting the transmission of any given pulse. After leaving the aperture, the number of overlapping pulses changes as the beam focuses or defocuses and a change in wind velocity such as beam slewing or stagnation will similarly alter the overlapping effect.

For laser propagation in the atmosphere, the appropriate form of Maxwell's electromagnetic wave equation is the paraxial approximation represented for the Nth pulse by

$$2iF\frac{\partial A^N}{\partial z} + \nabla^2 A^N + \frac{2F^2 z_f^2 (n_\infty - 1)}{R_m^2} \times \left(\frac{\rho-\rho_\infty}{\rho_\infty}\right)^N A^N = 0 \tag{2}$$

where

F = the Fresnel number $2\pi R_m^2/\lambda z_f$
A = the complex amplitude
z_f = the range to the focus
n_∞ = the ambient index of refraction

The amplitude distribution at the aperture is required as a boundary condition and an additional equation relating index of refraction to density is simply a linear expression.

Whereas the basic governing equations presented can be solved entirely by finite-difference methods, the requirements in computation time and computer storage are enormous. A particularly straightforward and efficient method of solution is to use Fourier transforms utilizing the Fast-Fourier Transform (FFT) algorithm.[3] This method is typically many times faster than ordinary finite differences and usually requires less computer storage. Because the air density is explicitly determined once the intensity distribution is known, it remains to solve the wave equation for the amplitude distribution then I is calculated from $I=AA^*$. The wave equation is solved by introducing a phase-front distortion term proportional to the density changes produced by heating, finite differencing in the propagation (z) direction, and taking the Fourier transform of the result thus giving

$$\overline{A^N_{k+1}} = \overline{A^N_k \exp(i\Delta\varphi)^N_k} \exp\left[\frac{-i\Delta z(p^2+q^2)}{2F}\right] \tag{3}$$

The barred quantities indicate FFT transformed values, φ is the distortion parameter; p and q are the transform variables

Presented as Paper 75-718 at the AIAA 10th Thermophysics Conference, Denver, Colo., May 27-29, 1975; submitted Aug. 4, 1976; revision received Oct. 29, 1976.

Index categories: Hydrodynamics; Lasers.

*Aerospace Engineer, Physical Sciences Directorate.
†Research Physicist, High Energy Laser Directorate.